

1
2 **Sensitivity of free tropospheric carbon monoxide to atmospheric weather states and**
3 **their persistency: an observational assessment over the Nordic countries**

4
5 Manu Anna Thomas¹ and Abhay Devasthale²

6
7 ¹Air quality unit, Research and development department, Swedish Meteorological and Hydrological
8 Institute (SMHI), Norrköping, Sweden

9 ²Atmospheric remote sensing unit, Research and development department, SMHI, Norrköping, Sweden

10
11 Corresponding author: manu.thomas@smhi.se

12
13
14 **Abstract**

15
16 Among various factors that influence the long-range transport of pollutants in the free troposphere
17 (FT), the prevailing atmospheric weather states probably play the most important role in governing
18 characteristics and efficacy of such transport. The weather states, such as a particular wind pattern,
19 cyclonic or anticyclonic conditions etc, and their degree of persistency determine the spatio-temporal
20 distribution and the final fate of the pollutants. This is especially true in the case of Nordic countries,
21 where baroclinic disturbances and associated weather fronts primarily regulate local meteorology, in
22 contrast to the lower latitudes where convective paradigm plays similar important role. Furthermore,
23 the long-range transport of pollutants in the FT has significant contribution to the total column burden
24 over the Nordic countries. However, there is insufficient knowledge on the large-scale co-variability of
25 pollutants in the FT and atmospheric weather states based solely on observational data over this region.
26 The present study attempts to quantify and understand this statistical co-variability while providing
27 relevant meteorological background.

28
29 To that end, we select eight weather states that predominantly occur over the Nordic countries and three
30 periods of their persistency (3-days, 5-days, and 7-days), thus providing in total 24 cases to investigate
31 sensitivity of free tropospheric carbon monoxide, an ideal tracer for studying pollutant transport, to
32 these selected weather states. The eight states include four dominant wind directions (namely, NW, NE,
33 SE and SW), cyclonic and anticyclonic conditions, and the enhanced positive and negative phases of

34 the North Atlantic Oscillation (NAO). For our sensitivity analysis, we use recently released Version 6
35 retrievals of CO at 500 hPa from the Atmospheric Infrared Sounder (AIRS) onboard Aqua satellite
36 covering 11-yr period from September 2002 through August 2013 and winds from the ECMWF's ERA-
37 Interim project to classify weather states for the same 11-yr period.

38

39 We show that, among the various weather states studied here, southeasterly winds lead to highest
40 observed CO anomalies (up to +8%) over the Nordic countries while transporting pollution from the
41 central and eastern parts of Europe. The second (up to +4%) and third highest (up to +2.5%) CO
42 anomalies are observed when winds are northwesterly (facilitating inter-continental transport from
43 polluted North American regions) and during the enhanced positive phase of the NAO respectively.
44 Higher than normal CO anomalies are observed during anticyclonic conditions (up to +1%) compared
45 to cyclonic conditions. The cleanest conditions are observed when winds are northeasterly and during
46 the enhanced negative phases of the NAO, when relatively clean Arctic air masses are transported over
47 the Nordic regions in the both cases. In case of nearly all weather states, the CO anomalies consistently
48 continue to increase or decrease as the degree of persistency of a weather state is increased. The results
49 of this sensitivity study further provide an observational basis for the process-oriented evaluation of
50 chemistry transport models, especially with regard to the representation of large-scale coupling of
51 chemistry and local weather states and its role in the long-range transport of pollutants in such models.

52

53

54

55

56

57

58

59

60

61

62

63

64

65

66

67

68 **1. Introduction**

69

70 Apart from the local sources of pollution that degrade local air quality and hence human health, many
71 studies show that, depending on the global and regional circulation patterns and favourable
72 meteorological conditions, the long range transport of pollutants also contributes to increased pollutant
73 concentrations. In fact, the importance of hemispheric and long range transport of pollutants is now
74 widely recognized in the scientific community, and the research focus in recent years has deservedly
75 been on better characterization of source-to-sink relationships and drivers of pollutant variability
76 during such transport (Li et al. 2002; Stohl et al. 2002; Creilson et al. 2003; Eckhardt et al. 2003; Trickl
77 et al. 2003; Duncan and Bay, 2004; Pfister et al. 2004; Huntrieser et al. 2005; Li et al. 2005; Chin et al.
78 2007; Shindell et al. 2008; Fiore et al. 2009; Dentener et al. 2010; Brandt et al. 2012; Christoudias et al.
79 2012; Lin et al. 2012). It is important to keep in mind that it is the local meteorology and synoptic scale
80 weather patterns that eventually determine the spatio-temporal distribution of pollutants, their transport
81 characteristics and final fate. One of the main mechanisms by which the pollutants (e.g. from wildfire
82 emissions) get transported from their source regions to the Earth's northern most latitudes as far as the
83 Arctic is through varying states of atmospheric circulation. This was first realized through the
84 phenomenon of Arctic haze observed during the winter/spring months that was first reported in the
85 1950s (Quinn et al. 2007). It is now known that the major pathways to the Arctic depend upon the
86 season and the position of the Arctic front. For example, during the winter and spring months, the
87 intense Siberian high pressure system pushes the Arctic front towards the south whereby the polluted
88 regions of the Eurasian subcontinent are within the Arctic airmass resulting in the efficient transport of
89 pollutants during this time of the year.

90

91 The spatio-temporal distribution of pollutants over the Nordic countries is a result of complex interplay
92 of local sources, atmospheric circulation patterns, and contributions from the long range transport
93 originating from North America, continental Europe and Asia. The dominant modes of atmospheric
94 variability in the northern hemisphere affecting the Nordic countries, especially in winter, are the North
95 Atlantic Oscillation (NAO) and Arctic Oscillation (AO). The positive and negative phases of NAO are
96 marked by changes in the wind speed and direction over the Atlantic, heat and moisture transport
97 across the Atlantic. The frequency and intensity of the number of storms and warm conveyor belts
98 influence the transatlantic transport of pollutants from North America to Europe, including over the
99 northern European latitudes (Li et al. 2002; Hurrell et al. 2003; Duncan and Bey, 2004; Dentener et al.

100 2010). Eckhardt et al. (2003) observed a strong correlation between the NAO and transport of
101 anthropogenic pollution into the Arctic and Eastern Europe from all the NH continents with an
102 enhanced transport during the positive NAO phase. However, a significant anti-correlation is observed
103 between NAO and the anthropogenic pollutants over western and central Europe (Christoudias et al.
104 2012). Significant correlations between the positive phase of AO and elevated ozone concentrations in
105 western Europe is observed and can be attributed largely to in-situ production associated with the
106 subsidence within the high pressure dome or entrainment of pollutants into this dome (Creilson et al.
107 2005). Pfister et al. (2004) showed that when averaged over Europe, almost 67% of the anthropogenic
108 carbon monoxide (CO) at the surface comes from regional sources, in addition to the transport from
109 North America (14%) and Asia (15%). However, at higher altitudes, the contribution from North
110 America and Asia is significantly higher. Brandt et al. (2012) using the 3D long range chemistry
111 transport hemispheric model showed that the contributions from North American anthropogenic
112 emissions to the ozone levels in European subcontinent is 3.1% and the contributions from European
113 anthropogenic sources to North America is 0.9%.

114

115 One of the major pathways carrying pollutants from the continental Europe to the Arctic passes over
116 the Nordic countries. Tang et al. (2009) studied the long range transport and weather patterns relating to
117 high ozone events in southern Sweden, and using a trajectory model showed that these events occurred
118 during anticyclonic events, especially during summer. But they observed strong negative relationship
119 between cyclonic and high ozone events. Recently, Devasthale and Thomas (2012) investigated co-
120 variation of temperature inversions and CO over Scandinavia during winter using satellite sensor data.
121 They showed that the increased levels of CO are observed when the atmosphere is thermodynamically
122 unstable (weaker or negative inversion strength) and when the westerly winds are strong. Apart from
123 long range transport of pollutants in the free troposphere (FT), in cold climate of the Nordic countries,
124 unfavorable meteorological conditions such as thermal inversions, low boundary layer height and low
125 temperatures can contribute to increased pollutant concentrations in the lowermost troposphere near the
126 surface. The above mentioned studies emphasize the need for a better quantification of the linkages
127 between the pollutant concentrations and atmospheric weather states.

128

129 Many of the studies mentioned above examine CO, since CO is often considered as an excellent tracer
130 to investigate pollution transport characteristics due to its moderate life-time in the atmosphere.
131 Increased carbon monoxide levels would not only enhance carbon dioxide levels in the atmosphere
132 through its reaction with hydroxyl (OH) radicals, but also indirectly increase concentrations of short-

133 lived climate pollutants such as ozone and methane, which would otherwise be depleted by OH
134 radicals. Therefore, monitoring CO and understanding its sensitivity to large-scale weather patterns,
135 based solely on observations, is important not only to gain insights into long range pollution transport,
136 but also to serve as an observational basis for the sensitivity studies to evaluate chemistry transport
137 models.

138
139 In spite of their importance as mentioned above, there is no consistent observationally based
140 assessment of how the dominant weather states impact free tropospheric CO variability over the Nordic
141 countries. The present study attempts to partially fill this gap. Decreased instrument sensitivity over
142 very cold surfaces, variable snow cover, difficulties in cloud detection etc are some of the factors that
143 limit the use of satellite remote sensing to study the atmospheric composition variability over the
144 Nordic regions, especially in the lowermost troposphere. But the data records of atmospheric
145 composition from satellite sensors, esp. from hyperspectral sounders such as IASI (Clerbaux et al.
146 2009) and AIRS (Chahine et al. 2006), are continuously improving and we now have better
147 understanding of their retrieval quality and sensitivities. More than a decade long data, e.g. from AIRS
148 and MOPITT, can be exploited to investigate statistics on the large-scale co-variability of weather
149 states and trace gases, as attempted here.

150
151 In the next section, we describe the data set used and methodology adopted, followed by presentation
152 of an overview of dominant atmospheric circulation patterns and corresponding meteorological
153 conditions over the Nordic region, with specific focus on Sweden, in Section 3. We then discuss
154 sensitivity of CO to these patterns and persistency of these patterns in Section 4. The final section
155 presents conclusions.

156 157 **2. The Atmospheric Infrared Sounder (AIRS) CO and ERA-Interim data sets**

158
159 AIRS onboard Aqua satellite has 2378 hyperspectral channels, out of which about 36 well-defined
160 channels with wavenumbers ranging from 2181.49 cm^{-1} to 2221.12 cm^{-1} are used in V6 to retrieve CO
161 ([http://disc.sci.gsfc.nasa.gov/AIRS/documentation/v6_docs/v6releasedocs-](http://disc.sci.gsfc.nasa.gov/AIRS/documentation/v6_docs/v6releasedocs-1/V6_Retrieval_Channel_Sets.pdf)
162 [1/V6_Retrieval_Channel_Sets.pdf](http://disc.sci.gsfc.nasa.gov/AIRS/documentation/v6_docs/v6releasedocs-1/V6_Retrieval_Channel_Sets.pdf)). A priori profiles (sets of 100 layers) with monthly granularity are
163 used to as a first guess. These profiles are based MOZART (Model for OZone And Related chemical
164 Tracers) monthly mean hemispheric profiles
165 ([http://disc.sci.gsfc.nasa.gov/AIRS/documentation/v6_docs/v6releasedocs-](http://disc.sci.gsfc.nasa.gov/AIRS/documentation/v6_docs/v6releasedocs-1/V6_Retrieval_Channel_Sets.pdf)

166 [1/V6_CO_Initial_Guess_Profiles.pdf](#)). By varying the geophysical state, the retrieval algorithm for CO
167 basically tries to minimize the weighted difference between clear-sky radiance and the radiance
168 computed using forward model. Using averaging kernels, the retrieval algorithm relates estimated CO
169 profile to “true” profile and a priori information. The algorithm details are described in Susskind et al.
170 (2003) and in Warner et al. (2007, 2010, and 2013).

171
172 We use recently released Version 6, daily standard and support Level 3 retrievals of CO (AIRS Science
173 Team/Joao Teixeira, 2013; AIRS-V6L3UG, 2013). Eleven years of data from September 2002 to and
174 including August 2013 are analysed. The AIRS retrievals of temperature and CO are validated and
175 matured considerably over the years to enable variability studies (Divakarla et al. 2006; Fetzer, 2006;
176 Warner et al., 2007; Yurganov et al. 2008; Warner et al. 2010; Warner et al. 2013). The accuracy and
177 biases of AIRS CO are well documented in the studies mentioned above.

178
179 Since the focus of the present study is on free troposphere, we have analysed CO at four different
180 vertical levels, namely 850hPa, 700hPa, 500hPa and 400hPa, but the results are shown only for
181 500hPa. The reasons for that are a) the signal of pollutant transport in the free troposphere is most
182 tangible at this level, b) coincidentally AIRS retrievals are of best quality at this level (Yurganov et al.
183 2008; Warner et al. 2010), and c) for the sake of brevity. The tendencies in CO observed at these four
184 vertical levels and corresponding wind patterns during selected weather states are not significantly
185 different, since many of the weather states, when they are persistent, affect the entire free troposphere
186 (as shown later).

187
188 We analyse AIRS retrievals only when the degrees of freedom value is larger than 0.5. For
189 investigating large-scale features and tendencies, as attempted in the present study, AIRS Level 3 CO
190 data are quite suitable as for example shown by Devasthale and Thomas (2012). Data from both
191 ascending and descending passes of the afternoon Aqua satellite are used. We have allowed up to 30%
192 cloud cover while analysing the AIRS CO retrievals based on the findings of our sensitivity studies
193 (Devasthale and Thomas, 2012) and previous experience with AIRS data (Devasthale et al. 2010;
194 Devasthale et al. 2011; Devasthale et al. 2012; Devasthale et al. 2013). Susskind et al (2003) have
195 previously presented detailed analysis of the accuracy of AIRS retrievals in presence of clouds. The
196 yield and accuracy of AIRS retrievals should not degrade significantly up to 30% cloud cover.
197 Recently, Warner et al. (2013) showed that the AIRS CO retrievals in cloud contaminated cases are of
198 comparable quality. The degrees of freedom of the signal, an indicator of information content, are

199 reduced only by up to 0.2 in cloudy cases (please refer Figs. 3 and 4 in Warner et al. 2013). The
200 difference should even be smaller in our cases, since we allow only 30% cloud contamination.
201 Furthermore, the majority of opaque clouds occurring over the study area are low clouds (cloud tops
202 less than 700 hPa). Since we analysed retrievals at 500 hPa, the cloud impact is estimated to be small.
203 Finally, the absence of any spatial correlation between cloud fraction and observed CO anomalies also
204 suggests that the cloud impact is negligible.

205
206 The advantage of using AIRS data lies in the fact that a) the simultaneous retrievals of temperature and
207 humidity in time and space are available which can be used to understand thermodynamical properties
208 of the atmosphere and possible transport of heat and moisture during different weather states, b) the
209 longest (>11yr) data record of CO from hyperspectral measurements is available, and c) the synergy
210 with other A-Train sensors providing aerosol and cloud information can be exploited in future studies.

211
212 For investigating winds, we used 6 hourly zonal (u) and meridional (v) wind components from the
213 ECMWF's ERA-Interim reanalysis (Dee et al. 2011) for the same period when AIRS CO data are
214 available.

215 216 **3. An overview of selected weather states**

217
218 In the present study, we select 8 weather states that most frequently occur over the study area (42N-
219 80N, 10W-40E). Figures 1-5 show an overview of circulation patterns and typical meteorological
220 conditions observed under these weather states. The states are selected based on the synthesis of
221 previous literature (e.g. Chen, 2000; Linderson, 2001) and further confirmed by manual inspection of
222 numerous weather reports from the Swedish Meteorological and Hydrological Institute. Since the
223 persistency of a weather state may enhance or reduce pollution levels in the free troposphere, for each
224 selected weather state, we have also investigated tendencies of CO anomalies under three persistency
225 periods, namely 3-days (P3), 5-days (P5) and 7-days (P7) respectively. For brevity, we present the
226 circulation patterns and meteorological conditions only for the P5 case, but the sensitivity results for
227 CO are shown for all weather states and persistency periods later in this study.

228
229 The eight identified weather states consist of four dominant wind directions (NW, NE, SE and SW),
230 anticyclonic and cyclonic conditions, and two enhanced phases of the NAO. In case of the first four
231 weather states, we chose the center (55N-60N, 12E-20E) of the study area (45N-80N, 10W-40E) to

232 average daily wind speed and direction at 850hPa from the ERA-Interim reanalysis. Based on these
233 daily averages we selected days when a particular wind direction prevailed and persisted for at least 3,
234 5 and 7 days. The same procedure is applied for selecting anticyclonic and cyclonic conditions based
235 on average mean sea level pressure (MSLP) over the center of the study region. For the remaining two
236 weather states, the selection of days is based on NAO indices. The overlapping dates among weather
237 states are intuitively avoided by the algorithm. For example, if a certain day is assigned to a certain
238 weather state, then that day is not considered further in the statistics of other weather states. But the
239 selected days are inclusive within the persistency periods of the same weather state. For example, when
240 a weather state persists for 7 consecutive days, then the first three and five days of such event are
241 included in the corresponding P3 and P5 cases. We analysed weather state data in the following order.
242 First, the time information for P3, P5, and P7 for the NAO cases are obtained, followed by the analysis
243 for anticyclonic and cyclonic conditions and finally for the wind directions (clockwise NW, NE, SE,
244 SW).

245
246 During the selected 11-yr study period, relatively speaking, these states (i.e. NW, NE, SE, SW,
247 anticyclonic and cyclonic, and EP and EN) occur 9%, 3%, 4%, 14%, 28%, 27%, 6% and 9% of the
248 time respectively. The number of events studied for each state is mentioned in Table 1. The probability
249 of a particular weather state prevailing over the study area decreases with increasing persistency.
250 Consequently, the results for 7-day periods, shown later, are in some cases patchy. However, the CO
251 anomalies exceed at least one standard deviation and hence are significant.
252 Figs. 1 and 2 show the composites of wind direction and strength at 850 hPa for the P5 case for much
253 broader area to better understand the pathways of the air masses entering the study area. The actual
254 stud area is marked by black rectangles.

255
256 When the winds are of NW origin, the air masses are transported from across the northernmost Atlantic
257 into the Nordic countries and Eastern Europe (Fig. 1a). This results in colder than average temperatures
258 and drier conditions in the eastern parts of the study area and warmer and moist conditions in the west
259 as reflected in Fig. 5 that shows the corresponding temperature anomalies. However, when the winds
260 have a NE component, the airmasses transported across the Atlantic from North America travel
261 northward almost perpendicular to the latitude belts up to 75N is merged with the Arctic air mass and
262 merges with the anticyclonic flow with the center of this flow located over southern Norway (Fig. 1b).
263 This anticyclonic flow further transports heat from the continental Europe and eastern Atlantic over the
264 Norwegian Sea as visible in Fig. 5. In the SW case, it can be seen that the air masses that travel to

265 Scandinavia likely originate from a much higher trajectory (north of 50N) in North America and are
266 mixed with east Atlantic gyre (Fig. 2a). The warm winds from the southerly latitudes (in comparison to
267 the NW case) cause warming of the middle troposphere over much of the eastern study area (Fig. 5).
268 The anticyclonic flow centered over Finland in the SE case draws in warm airmasses from the central
269 and eastern parts of Europe (Fig. 2b) also resulting in warmer temperatures (Fig. 5).

270

271 Another important characteristic of the Earth's atmosphere is pressure distribution as it defines the wind
272 and weather patterns globally. Fig. 3 shows the composites of the magnitude and wind direction at 850
273 hPa during high MSLP conditions and low MSLP conditions over the center of the study. During high
274 MSLP conditions, the winds seem to favour the transatlantic transport towards the northernmost
275 latitudes. The anticyclonic flow further circulates airmasses from the continental Europe to over
276 Norwegian Sea and the northern parts of the study area. On the other hand during low MSLP
277 conditions, the winds have a much lower trajectory in the Atlantic and the air masses advected from
278 across the Atlantic are transported over continental Europe and are caught up in the cyclonic flow
279 centered around central Scandinavia. The circulation pattern during anticyclonic (cyclonic) conditions
280 leads to enhanced (reduced) heat and moisture transport over the western part of Scandinavia and
281 northeast Atlantic Ocean as shown in Fig. 5.

282

283 The gradients in pressure and hence, the winds, force different types of oscillations. One such
284 prominent oscillation, manifested in boreal winter as a see-saw in pressure over the Atlantic, is the
285 North Atlantic Oscillation. As described in the introduction, the NAO phases play an important role in
286 the transatlantic transport of pollutants. Shown in Fig. 4 are respectively the 850 hPa winds associated
287 with enhanced positive (EP: NAO index $> +1$) and enhanced negative NAO conditions (EN: NAO
288 index < -1) and when these conditions prevail for at least five consecutive days. The daily NAO index
289 for the period in study was downloaded from the following link
290 <http://www.cpc.ncep.noaa.gov/products/precip/CWlink/pna/nao.shtml>. The NAO index itself does not
291 show any significant trend during the last decade as shown in the Supplementary Figure S1.

292

293 During the enhanced positive NAO phase, the winds are stronger and there is a significant advection of
294 air masses across the Atlantic from northern US and Canada into northern Europe and Scandinavia
295 (Fig. 4a). In fact, there is striking resemblance between warmer temperature anomalies (Fig. 5) and
296 wind pattern in the EP case, suggesting the efficiency of atmospheric transport. During the EN phase,
297 the winds are much weaker (Fig. 4b) and the cold Arctic air masses propagate into Scandinavian

298 countries (also clearly visible in Fig. 5) and there is a relatively stronger south westerly flow over
299 northern Europe.

300

301 The normalized frequency of number of days of data available for each weather state as function of
302 months is shown in Fig. 6. The distribution of their occurrence is not always uniform as expected, since
303 different weather states are dominant during different times of a year except for anticyclonic and
304 cyclonic periods (i.e. during above normal and below normal MSLP conditions) when their
305 occurrences are distributed evenly. The frequency distribution of EP and EN phases is such that the
306 enhanced positive NAO phases more prominent during the winter half of the year, while enhanced
307 negative NAO phases during the other half of the year. This unequal distribution of samples as a
308 function of months makes it difficult to compare their relative impact of weather states on observed CO
309 levels due to interference of seasonality of CO. To address this, we calculate 11-yr annual climatology
310 of CO by taking a weighted average based on the distribution of occurrence for a particular state as a
311 function of month as follows.

$$312 \quad C = \sum_{i=1}^{12} w_i * c_i \quad (1)$$

313 where i is month, w_i is monthly weight (based on figure shown above), c_i is monthly
314 climatology of CO.

315 We then subtract this climatology from the composite of CO observed under that state to compute
316 anomalies. This ensures that we remove the seasonal variations while comparing different states and
317 that the observed CO anomalies are indeed due to contribution from that particular weather state and its
318 persistency.

319

320 **4. Sensitivity of CO to weather states and their persistency**

321

322 The sources of CO over the study are mainly anthropogenic resulting from fossil fuel burning,
323 vehicular emissions and industrial activities. The biomass burning (natural and anthropogenic) also
324 contributes to the total CO budget. The seasonality in photochemical production and loss gains
325 importance with increasing altitude. This in combination with long-range and inter-continental
326 transport drives the seasonal variability of CO in the free troposphere over the study area. The
327 climatological seasonal distribution of CO at 500 hPa **over the study area** is shown in the
328 Supplementary Figure S2. As expected the CO concentrations are higher in the late winter to early
329 spring due to their increased lifetime as the photochemical loss is at its minimum because of the lack of

330 sunlight, and due to increased emissions and efficient transport during this time of the year.

331

332 Fig. 7 shows CO anomalies in the free troposphere (500 hPa) for four chosen wind directions and
333 persistency periods of P3, P5 and P7. Only statistically significant anomalies exceeding one standard
334 deviation are shown. When the winds are NW, above normal CO concentrations are observed over
335 northern Europe and CO anomalies increase significantly from P3 to P7. The examination of
336 circulation patterns and meteorological conditions for this weather state suggests that the NW air
337 masses may efficiently transport pollutants from across the Atlantic into the study region. The wind
338 speed also increases from P3 to P7. However, a different picture is observed when the winds are from
339 NE directions. In the P3 case, CO concentrations are much higher towards central Europe compared to
340 the Nordic countries. As the persistency of NE winds increases (from P3 to P7), reduced CO levels are
341 observed and the FT becomes comparatively clean. This can be explained by the fact that the
342 transatlantic pollutants that assimilate into the cyclonic flow observed during the NE cases are diluted
343 by the even stronger and cleaner Arctic air mass intrusions into Scandinavia under P7 period. When the
344 winds are SE, as mentioned before, the major pathway of pollution transport into the Nordic countries
345 is from central and Eastern Europe, as seen in Fig. 2. Comparatively much lower CO anomalies are
346 observed when the winds are SW. This may be because the air masses that travel to northern Europe
347 have their source regions from northern North American subcontinent (north of 45 N) which is
348 comparatively cleaner than the air masses from other wind directions. The southwesterly winds are
349 further mixed with cleaner air masses by the Atlantic gyre.

350

351 The deviation of the CO concentrations under anticyclonic and cyclonic conditions and their
352 persistency is shown in Fig. 8. The CO concentrations are in general higher over northern Europe
353 during anticyclonic conditions compared to cyclonic. The CO concentrations continue to increase as
354 anticyclonic conditions persist, and vice versa for cyclonic situations. A careful analysis of wind
355 patterns reveal that, during anticyclonic conditions, the polluted air masses from continental Europe
356 and North America are being drawn and circulated over the Nordic regions whereas, during cyclonic
357 conditions, cleaner Arctic air is mixed in the circulation gyre thereby being more efficient in the
358 removal and dispersal of pollutants resulting in relatively cleaner conditions.

359

360 Lastly, the sensitivity of CO to NAO phases and their persistency is shown in Fig. 9. The CO anomalies
361 are higher during the EP phase compare to the EN phase during all persistency periods. Furthermore,
362 there is clear tendency that, as the positive phases of the NAO persist, CO concentrations tend to

363 increase, especially in the higher latitudes. The free troposphere on the other hand becomes cleaner
364 when the negative phases of NAO persist. When the westerlies are weakened, cold and clean Arctic air
365 is drawn over the northern Europe during the negative phase. The tendencies in CO observed during
366 positive and negative phases of NAO are consistent with previous studies that use models simulations
367 (Eckhardt et al. 2003; Christoudias et al. 2012). For example, from the analysis of 15-year simulations,
368 Eckhardt et al. (2003) show enhanced tracer transport to the Arctic that passes over the Nordic
369 countries during positive phases of the NAO. Christoudias et al. (2012) also arrive at similar
370 conclusion with regard to transport towards northern Europe.

371

372 To quantify the importance of the different synoptic states, Fig. 10 shows the percentage change in CO
373 at free troposphere observed during the different weather states and persistency periods over the study
374 area. It can be seen that in nearly all the cases, the CO concentrations either steadily increased or
375 decreased with increased persistency of each weather state. The highest CO contribution, almost 4-8%
376 depending on the degree of persistency, is observed when the winds had a south-easterly component.
377 The second (up to 4%) and third highest (2.5%) anomalies are observed under NW winds and the
378 enhanced positive phases of the NAO respectively. The CO anomalies of completely opposite signs
379 during positive and negative phases of the NAO confirm the significance of the role of natural
380 variability in pollutant transport and diffusion. The anticyclonic and cyclonic conditions also show
381 opposite signs of CO anomalies, with maximum anomalies in the order of 1% observed during
382 anticyclonic conditions. The remaining weather states discussed in this study are more efficient in
383 reducing the build up of CO concentrations in the free troposphere, thereby lead to cleaner conditions.
384 It is to be kept in mind that these percentage changes in FT CO are based on averages and that the
385 individual short-term intrusion of pollution or strong but short-lived episodic transport can lead to
386 much higher changes in CO over the study area.

387

388 As mentioned earlier in Section 2, although we show results of CO variability at 500 hPa, we have
389 investigated this variability at four different levels in the free troposphere and in the total column CO as
390 well. As the persistency period of the chosen weather states increases, they are expected to affect the
391 CO variability in the entire troposphere in a systematic manner. This is evident in the Supplementary
392 Figure S3 that shows an example of the impact of wind directions on the total column CO variability.
393 The tendencies in CO total column anomalies under different wind directions and across persistency
394 periods are strikingly similar to those observed at 500 hPa. This underscores the importance of chosen
395 weather states in regulating CO variability *in the entire troposphere*. Under certain conditions, for

396 example very cold winters and surfaces, the sensitivity and information content of AIRS may peak only
397 in the middle troposphere and the total column values are affected by this problem. But keeping in
398 mind that our samples are spread across the entire year (not just in winter months) and that the
399 tendencies in CO anomalies are corroborated by wind and temperature anomaly patterns, it is most
400 likely that the results shown in Fig. S3 are realistic.

401

402 Finally, it must be mentioned that there are two mechanisms that are not considered in the present study
403 while interpreting the results. They are deep convection and warm conveyor belts (Madonna et al.
404 2014), both of which will lead to rapid transport of pollutants and thus are likely to contribute to the
405 observed anomalies. We argue that the impact of the convective mixing is minimal due to following
406 reasons. Firstly, the boundary layer is decoupled from the free troposphere most of the year due to
407 presence of inversions over the study region (Devasthale and Thomas, 2012). Then the likelihood of
408 strong episodic vertical injections of pollutants exists only during summer months (via dry or moist
409 convection), but it is very small since such events are usually few in number. And finally, in the free
410 troposphere (850-400 hPa), the atmospheric variability over the study region is governed by the large-
411 scale frontal systems created by the baroclinic disturbances (esp. in the winter half of the year). These
412 systems provide conducive environment for the advective rather than the local convective transport.
413 Our study area is usually at the receiving end of such systems that often arrive from the neighbouring
414 oceanic areas (Northeast Atlantic, North Sea, or the Arctic Ocean) or from the continental Europe.

415

416 The other transport mechanism, i.e. warm conveyor belts, will intrinsically be included in some of the
417 weather states studied here, especially in those cases where winds have history over the North Atlantic.
418 But it should be noted that, irrespective of the mechanism that triggered the transport of pollutants from
419 the source regions, it is the local weather state over our study area that will regulate the distribution of
420 these pollutants. For example, a particular weather state may either dampen the isentropic transport of
421 pollutants or facilitate it further to other regions (e.g. to the Arctic). For investigating the possible
422 impact of warm conveyor belts on the observed pollutant variability, we need to take into account full
423 transport history from the source to the study area. This is currently being addressed in a separate study.

424

425

426

427

428

429 **5. Conclusions**

430

431 Although the long-range transport governs the variability of pollutants in the free troposphere over the
432 Nordic countries, it is the atmospheric weather states that finally determine the spatio-temporal
433 distribution and the fate of the pollutants. The persistency of a particular weather state may further
434 enhance or reduce concentrations of pollutants. Understanding statistical link between weather states
435 and pollution variability is not only crucial to understand the role of long-range transport itself, but
436 also, be able to simulate such a link in chemistry transport models. The latter is important since CTMs
437 are often used to estimate changes in pollution load, attribution studies and developing mitigation
438 strategies under different climate change scenarios. In this context, the present study attempts to
439 provide insights into sensitivity of free tropospheric carbon monoxide to different weather states and
440 their degree of persistency based solely on observational data.

441

442 We investigated free tropospheric CO variability during eight weather states often prevailing over the
443 Nordic countries. Selected states include four wind directions (NW, NE, SE, and SW), anticyclonic and
444 cyclonic conditions, and positive and negative phases of the NAO. Furthermore, we investigated
445 tendencies in CO under three different degrees of persistency (3-day, 5-day and 7-day) of each weather
446 state. For nearly all the weather states, CO levels consistently continued to increase or decrease as the
447 degree of their persistency increased. Among the weather states studied here, relatively speaking, the
448 highest CO anomalies were observed when winds had southeasterly component, transporting pollutants
449 from the central and eastern European regions to over the Nordic countries. The second largest
450 contribution was from the northwesterly winds, most likely carrying pollutants as a result of long-range
451 transport from polluted North-American regions. The third largest anomalies are observed during
452 enhanced positive phase of the North Atlantic Oscillation, confirming the importance of this natural
453 variability in controlling pollutant distribution and transport over the study region. The cleanest
454 conditions were observed under prevailing northeasterly winds and the enhanced negative phase of the
455 NAO. The results from this sensitivity study provide an observational foundation for the process-
456 oriented evaluation of chemistry transport models.

457

458 It must be mentioned that although we provide relevant information on atmospheric circulation and
459 meteorology while inferring the potential role of long-range pollution transport in the observed
460 sensitivity of CO to weather states, the actual attribution and precise quantification of contribution from
461 different transport pathways must be done using trajectory or chemistry transport models.

462

463 **Acknowledgements**

464 We gratefully acknowledge the AIRS Science Team and NASA GES DISC for providing CO retrievals.
465 The wind data from ERA-Interim reanalysis have been obtained from the ECMWF Data Server. We
466 thank the three anonymous referees and the editor, Heini Wernli, for their constructive comments and
467 suggestions to improve the manuscript. M. T. acknowledges the funding support from the Monitoring
468 Atmospheric Composition and Climate Phase II (MACC-II) project and A. D. is thankful to Swedish
469 National Space Board (Rymdstyrelsen) for the funding support.

470

471

472 **References:**

473 AIRS Science Team/Joao Teixeira, *Aqua AIRS Level 3 Daily Standard Physical Retrieval*
474 (*AIRS+AMSU*), version 006, Greenbelt, MD, USA:NASA Goddard Earth Science Data and Information
475 Services Center (GES DISC), Accessed Oct 2013, doi:10.5067/AQUA/AIRS/DATA301, 2013.

476

477 AIRS-V6L3UG: AIRS Version 6 Level 3 data user guide, Edited by Baijun Tian, JLP/NASA, pp. 1-37,
478 2013 (available at: [http://disc.sci.gsfc.nasa.gov/AIRS/documentation/v6_docs/v6releasedocs-
479 1/V6_L3_User_Guide.pdf](http://disc.sci.gsfc.nasa.gov/AIRS/documentation/v6_docs/v6releasedocs-1/V6_L3_User_Guide.pdf)).

480

481 Brandt, J., Silver, J. D., Frohn, L. M., Geels, C., Gross, A., Hansen, A. B., Hansen, K. M., Hedegaard,
482 G. B., Skjøth, C. A., Villadsen, H., Zare, A., and Christensen, J. H.: An integrated model study for
483 Europe and North America using the Danish Eulerian Hemispheric Model with focus on
484 intercontinental transport, *Atmos. Environ.*, 53, 156–176, doi:10.1016/j.atmosenv.2012.01.011, 2012.

485

486 Chahine, M. T., Pagano, T. S., Aumann, H. H., Atlas, R., Barnet, C., Blaisdell, J., Chen, L., Divakarla,
487 M., Fetzer, E. J., Goldberg, M., Gautier, C., Granger, S., Hannon, S., Irion, F. W., Kakar, R., Kalnay, E.,
488 Lambigtsen, B. H., Lee, S.-Y., Le Marshall, J., McMillan, W. W., McMillin, L., Olsen, E. T.,
489 Revercomb, H., Rosenkranz, P., Smith, W. L., Staelin, D., Strow, L. L., Susskind, J., Tobin, D., Wolf,
490 W., and Zhou, L.: AIRS: Improving Weather Forecasting and Providing New Data on Greenhouse
491 Gases, *Bull. Am. Meteorol. Soc.*, 87, 911–926, 2006.

492

493 Chen, D., A monthly circulation climatology for Sweden and its application to a winter temperature
494 case study. *Int. J. Climatology*, 20, 1067-1076, 2000.

495

496 Chin, M., T. Diehl, P. Ginoux, and W. Malm, Intercontinental transport of pollution and dust aerosols:
497 implications for regional air quality, *Atmos. Chem. Phys.*, 7, 5501-5517, 2007.

498

499 Christoudias, T., Pozzer, A., and Lelieveld, J.: Influence of the North Atlantic Oscillation on air
500 pollution transport, *Atmos. Chem. Phys.*, 12, 869–877, 2012.

501

502 Clerbaux, C., Boynard, A., Clarisse, L., George, M., Hadji-Lazaro, J., Herbin, H., Hurtmans, D.,
503 Pommier, M., Razavi, A., Turquety, S., Wespes, C., and Coheur, P.-F.: Monitoring of atmospheric
504 composition using the thermal infrared IASI/MetOp sounder, *Atmos. Chem. Phys.*, 9, 6041-6054,
505 doi:10.5194/acp-9-6041-2009, 2009.

506

507 Creilson, J. K., Fishman, J., and Wozniak, A. E.: Intercontinental transport of tropospheric ozone: a
508 study of its seasonal variability across the North Atlantic utilizing tropospheric ozone residuals and its
509 relationship to the North Atlantic Oscillation, *Atmos. Chem. Phys.*, 3, 2053–2066, doi:10.5194/acp-3-
510 2053-2003, 2003.

511

512 Dee, D. P., Uppala, S. M., Simmons, A. J., Berrisford, P., Poli, P., Kobayashi, S., Andrae, U.,
513 Balmaseda, M. A., Balsamo, G., Bauer, P., Bechtold, P., Beljaars, A. C. M., van de Berg, L., Bidlot, J.,
514 Bormann, N., Delsol, C., Dragani, R., Fuentes, M., Geer, A. J., Haimberger, L., Healy, S. B., Hersbach,
515 H., Hólm, E. V., Isaksen, L., Kållberg, P., Köhler, M., Matricardi, M., McNally, A. P., Monge-Sanz, B.
516 M., Morcrette, J.-J., Park, B.-K., Peubey, C., de Rosnay, P., Tavolato, C., Thépaut, J.-N. and Vitart, F.:
517 The ERA-Interim reanalysis: configuration and performance of the data assimilation system. *Q.J.R.*
518 *Meteorol. Soc.*, 137: 553–597. doi: 10.1002/qj.828, 2011.

519

520 Dentener, F., Keating, T., and Akimoto, H. (Eds.): *Hemispheric Transport of Air Pollution*, United
521 Nations, ISBN: 978-92-1-117043-6, 2010.

522

523 Devasthale, A., and Thomas, M. A.: An investigation of statistical link between inversion strength and
524 carbon monoxide over Scandinavia in winter using AIRS data, *Atmospheric Environment*,
525 doi:10.1016/j.atmosenv.2012.03.042, 2012.

526

527 Devasthale, A., Sedlar, J., Koenigk, T., and Fetzer, E. J.: The thermodynamic state of the Arctic

528 atmosphere observed by AIRS: comparisons during the record minimum sea ice extents of 2007 and
529 2012, *Atmos. Chem. Phys.*, 13, 7441-7450, doi:10.5194/acp-13-7441-2013, 2013.

530

531 Devasthale, A., Tjernström, M., Caian, M., Thomas, M. A., Kahn, B. H., and Fetzer, E. J.: Influence of
532 the Arctic Oscillation on the vertical distribution of clouds as observed by the A-Train constellation of
533 satellites, *Atmos. Chem. Phys.*, 12, 10535-10544, doi:10.5194/acp-12-10535-2012, 2012.

534

535 Devasthale, A., Sedlar, J., and Tjernström, M.: Characteristics of water-vapour inversions observed
536 over the Arctic by Atmospheric Infrared Sounder (AIRS) and radiosondes, *Atmos. Chem. Phys.*, 11,
537 9813-9823, doi:10.5194/acp-11-9813-2011, 2011.

538

539 Devasthale, A., U. Willen, K.-G. Karlsson, and C. G. Jones, Quantifying the clear-sky temperature
540 inversion frequency and strength over the Arctic Ocean during summer and winter seasons from AIRS
541 profiles, *Atmos. Chem. Phys.*, 10, 5565-5572, 2010.

542

543 Divakarla, M. G., C. D. Barnet, M. D. Goldberg, L. M. McMillin, E. Maddy, W. Wolf, L. Zhou, and X.
544 Liu, Validation of Atmospheric Infrared Sounder temperature and water vapor retrievals with matched
545 radiosonde measurements and forecasts, *J. Geophys. Res.*, 111, D09S15, doi:10.1029/2005JD006116,
546 2006.

547

548 Duncan, B.N. and I. Bey, A Modeling Study of the Export Pathways of Pollution from Europe:
549 Seasonal and Interannual Variations (1987-1997), *J. Geophys. Res.*, doi:10.1029/2003JD004079,2004.

550

551 Eckhardt, S., Stohl, A., Beirle, S., Spichtinger, N., James, P., Forster, C., Junker, C., Wagner, T., Platt,
552 U., and Jennings, S. G.: The North Atlantic Oscillation controls air pollution transport to the Arctic,
553 *Atmos. Chem. Phys.*, 3, 1769–1778, doi:10.5194/acp-3-1769-2003, 2003.

554

555 Fetzer, E. J.: Preface to special section: Validation of Atmospheric Infrared Sounder Observations, *J.*
556 *Geophys. Res.*, 111, D09S01, doi:10.1029/2005JD007020, 2006.

557

558 Fiore, A. M., F.J. Dentener, O. Wild, C. Cuvelier, M.G. Schultz, P. Hess, C. Textor, M. Schulz, R.M.
559 Doherty, L.W. Horowitz, I.A. MacKenzie, M.G. Sanderson, D.T. Shindell, D.S. Stevenson, S. Szopa, R.
560 Van Dingenen, G. Zeng, C. Atherton, D. Bergmann, I. Bey, G. Carmichael, W.J. Collins, B.N. Duncan,

561 G. Faluvegi, G. Folberth, M. Gauss, S. Gong, D. Hauglustaine, T. Holloway, I.S.A. Isaksen, D.J. Jacob,
562 J.E. Jonson, J.W. Kaminski, T.J. Keating, A. Lupu, E. Marmer, V. Montanaro, R.J. Park, G. Pitari, K.J.
563 Pringle, J.A. Pyle, S. Schroeder, M.G. Vivanco, P. Wind, G. Wojcik, S. Wu, and A. Zuber, Multimodel
564 estimates of intercontinental source-receptor relationships for ozone pollution. *J. Geophys. Res.*, 114,
565 D04301, doi:10.1029/2008JD010816, 2009.

566

567 Huntrieser, H., Heland J., Schlager H., Forster C., Stohl A., Aufmhoff H., Arnold F., Scheel H. E.,
568 Campana M., Gilge S., Eixmann R., and O. Cooper, Intercontinental air pollution transport from North
569 America to Europe: Experimental evidence from airborne measurements and surface observations.
570 *Journal of Geophysical Research*, 110(D01305), doi: 10.1029/2004JD005045, 2005.

571

572 Hurrell, J. W., Kushnir, Y., Ottersen, G., and Visbeck, M.: An Overview of the North Atlantic
573 Oscillation, in: *The North Atlantic Oscillation: Climatic Significance and Environmental Impact*, edited
574 by: Hurrell, J. W., Kushnir, Y., Ottersen, G., and Visbeck, M., 1–35, *Geophysical Monograph*, 2003.

575

576 Li, Q., Jacob, D. J., Bey, I., Palmer, P. I., Duncan, B. N., Field, B. D., Martin, R. V., Fiore, A. M.,
577 Yantosca, R. M., Parrish, D. D., Simmonds, P. G., and Oltmans, S. J.: Transatlantic transport of
578 pollution and its effects on surface ozone in Europe and North America, *J. Geophys. Res.*, 107, ACH 4,
579 doi:10.1029/2001Jd001422, 2002.

580

581 Li, Q., and co-authors: Convective outflow of South Asian pollution: A global CTM simulation
582 compared with EOS MLS observations. *Geophys. Res. Lett.*, 32, L14826, doi:10.1029/
583 2005GL022762, 2005.

584

585 Lin, M., A. Fiore, L. W. Horowitz, O. R. R. Cooper, V. Naik, J. S. Holloway,
586 B. J. J. Johnson, A. M. Middlebrook, S. J. J. Oltmans, I. B. Pollack, T. B. Ryerson, J.
587 Warner, C. Wiedinmyer, J. Wilson, and B. Wyman, Transport of Asian ozone pollution into surface air
588 over the western United States in spring, *J. Geophys. Res.*, 117, D00V07, doi:10.1029/2011JD016961,
589 2012.

590

591 Linderson M-J., Objective classification of atmospheric circulation over Southern Scandinavia. *Int. J.*
592 *Climatology*, 21, 155-169, 2001.

593 Madonna, E., H. Wernli, H. Joos, and O. Martius, Warm Conveyor Belts in the ERA-Interim Dataset
594 (1979–2010). Part I: Climatology and Potential Vorticity Evolution. *J. Climate*, 27, 3–26. doi:
595 <http://dx.doi.org/10.1175/JCLI-D-12-00720.1>, 2014.

596 Pfister, G., G. Petron, L. K. Emmons, J. C. Gille, D. P. Edwards, J.-F. Lamarque, J.-L. Attie, C. Granier,
597 and P. C. Novelli: Evaluation of CO simulations and the analysis of the CO budget for Europe, *J.*
598 *Geophys. Res.*, 109, D19304, doi:10.1029/2004JD004691, 2004.

599 Quinn, P. K., Shaw, G., Andrews, E., Dutton, E. G., Ruoho-Airola, T., Gong, S. L.: Arctic Haze: Current
600 trends and knowledge gaps, *Tellus*, 59B, 99–114, doi: 10.1111/j.1600-0889.2006.00238.x, 2007.

601 Shindell, D.T., M. Chin, F. Dentener, R.M. Doherty, G. Faluvegi, A.M. Fiore, P. Hess, D.M. Koch, I.A.
602 MacKenzie, M.G. Sanderson, M.G. Schultz, M. Schulz, D.S. Stevenson, H. Teich, C. Textor, O. Wild,
603 D.J. Bergmann, I. Bey, H. Bian, C. Cuvelier, B.N. Duncan, G. Folberth, L.W. Horowitz, J. Jonson, J.W.
604 Kaminski, E. Marmer, R. Park, K.J. Pringle, S. Schroeder, S. Szopa, T. Takemura, G. Zeng, T.J.
605 Keating, and A. Zuber, A multi-model assessment of pollution transport to the Arctic. *Atmos. Chem.*
606 *Phys.*, 8, 5353-5372, doi:10.5194/acp-8-5353-2008, 2008.

607 Stohl, A., Eckhardt S., Forster C., James P., and P. Spichtinger, On the pathways and timescales of
608 intercontinental air pollution transport. *Journal of Geophysical Research* 107(D23), 4684,
609 doi:10.1029/2001JD001396, 2002.

610

611 Susskind, J., C. Barnet, and J. Blaisdell, Retrieval of Atmospheric and Surface Parameters from
612 AIRS/AMSU/HSB Data in the Presence of Clouds *IEEE Transactions on Geoscience and Remote*
613 *Sensing*, 41(2), 390-409, 2003.

614

615 Tang, L., Karlsson, P. E., Gu, Y., Chen, D., Grennfelt, P.: Synoptic weather types and long-range
616 transport patterns for ozone precursors during high-ozone events in Southern Sweden, *Ambio*, 38, 459–
617 464, 2009.

618

619 Trickl, T., O. R. Cooper, H. Eisele, P. James, R. Mücke, and A. Stohl, Intercontinental transport and its
620 influence on the ozone concentrations over central Europe: Three case studies. *Journal of Geophysical*

621 Research 108(D12), 8530, doi:10.1029/2002JD002735, 2003.

622

623 Warner, J. X., Comer, M. M., Barnet, C. D., McMillan, W. W., Wolf, W., Maddy, E., and Sachse, G.: A
624 comparison of satellite tropospheric carbon monoxide measurements from AIRS and MOPITT during
625 INTEX-A, *J. Geophys. Res.*, 112, doi:10.1029/2006JD007925, 2007.

626

627 Warner, J., Carminati, F., Wei, Z., Lahoz, W., and Attié, J.-L.: Tropospheric carbon monoxide
628 variability from AIRS under clear and cloudy conditions, *Atmos. Chem. Phys.*, 13, 12469-12479,
629 doi:10.5194/acp-13-12469-2013, 2013.

630

631 Warner, J. X., Wei, Z., Strow, L. L., Barnet, C. D., Sparling, L. C., Diskin, G., and Sachse, G., Improved
632 agreement of AIRS tropospheric carbon monoxide products with other EOS sensors using optimal
633 estimation retrievals, *Atmospheric Chemistry and Physics* 10, 9521-9533, doi:10.5194/acp-10-9521-
634 2010, 2010.

635

636 Yurganov, L. N., W. W. McMillan, A. V. Dzhola, E. I. Grechko, N. B. Jones, and G. R. van der Werf,
637 Global AIRS and MOPITT CO measurements: Validation, comparison, and links to biomass burning
638 variations and carbon cycle. *Journal of Geophysical Research* 113, D09301,
639 doi:10.1029/2007JD009229, 2008.

640

641

642

643

644

645

646

647

648

649

650

651

652

653

	P3	P5	P7
NW	180	72	26
NE	85	31	11
SE	63	25	9
SW	280	100	38
Anticyclonic	556	224	74
Cyclonic	540	218	78
EP	121	48	17
EN	178	72	25

654

655 Table 1: The number of events studied for each of the weather state and its persistency.

656

657

658

659

660

661

662

663

664

665

666

667

668

669

670

671

672

673

674

675

676

677

678

679

680

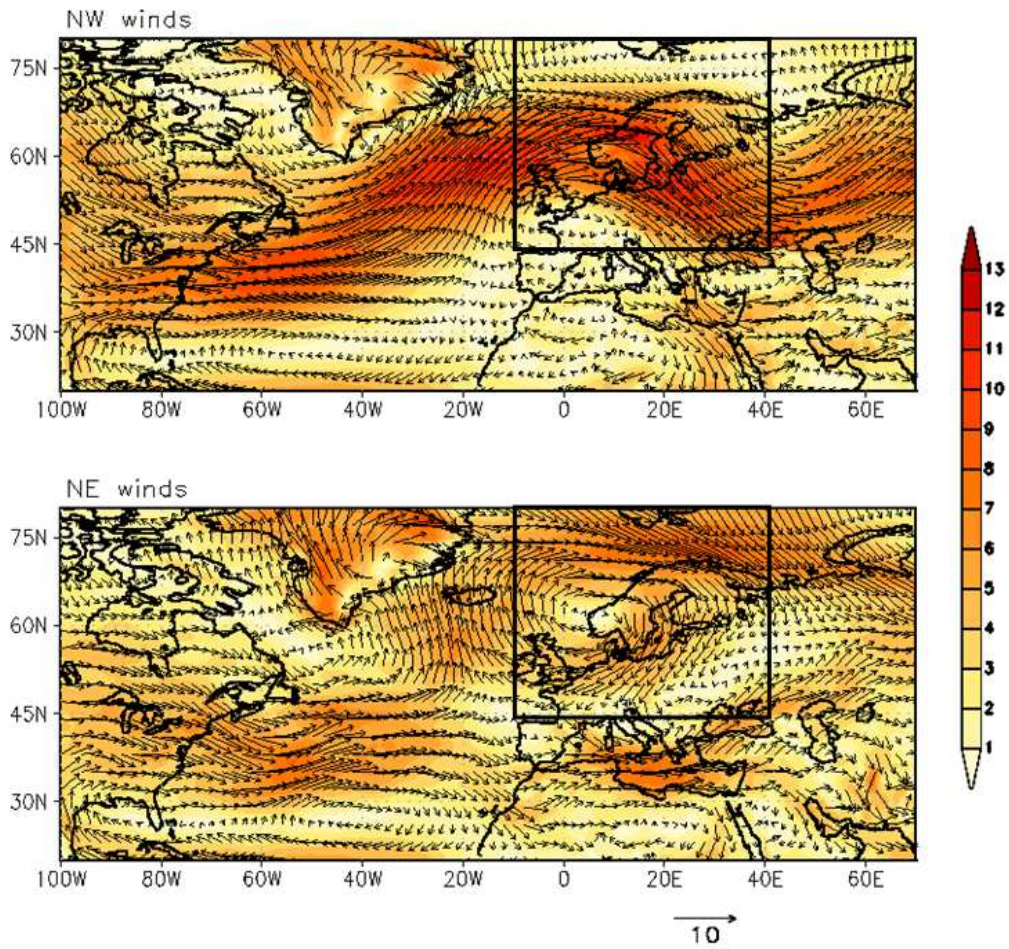
681

682

683

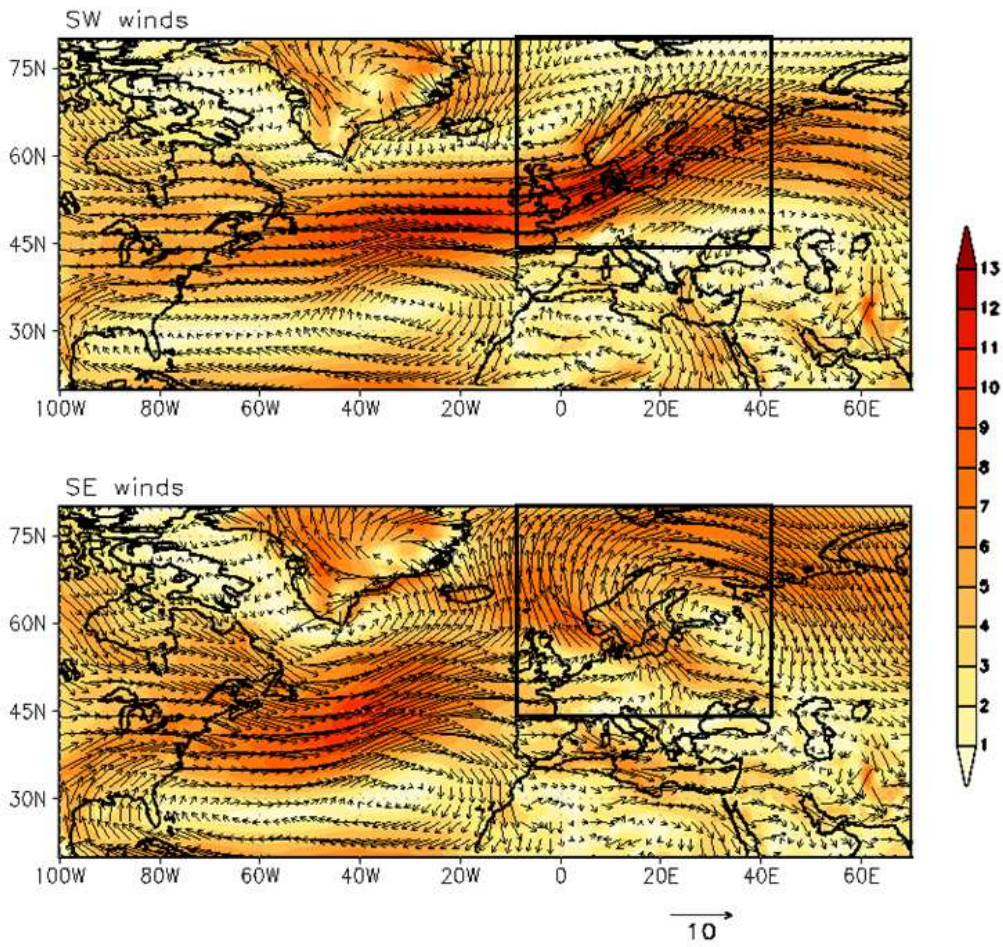
684

685



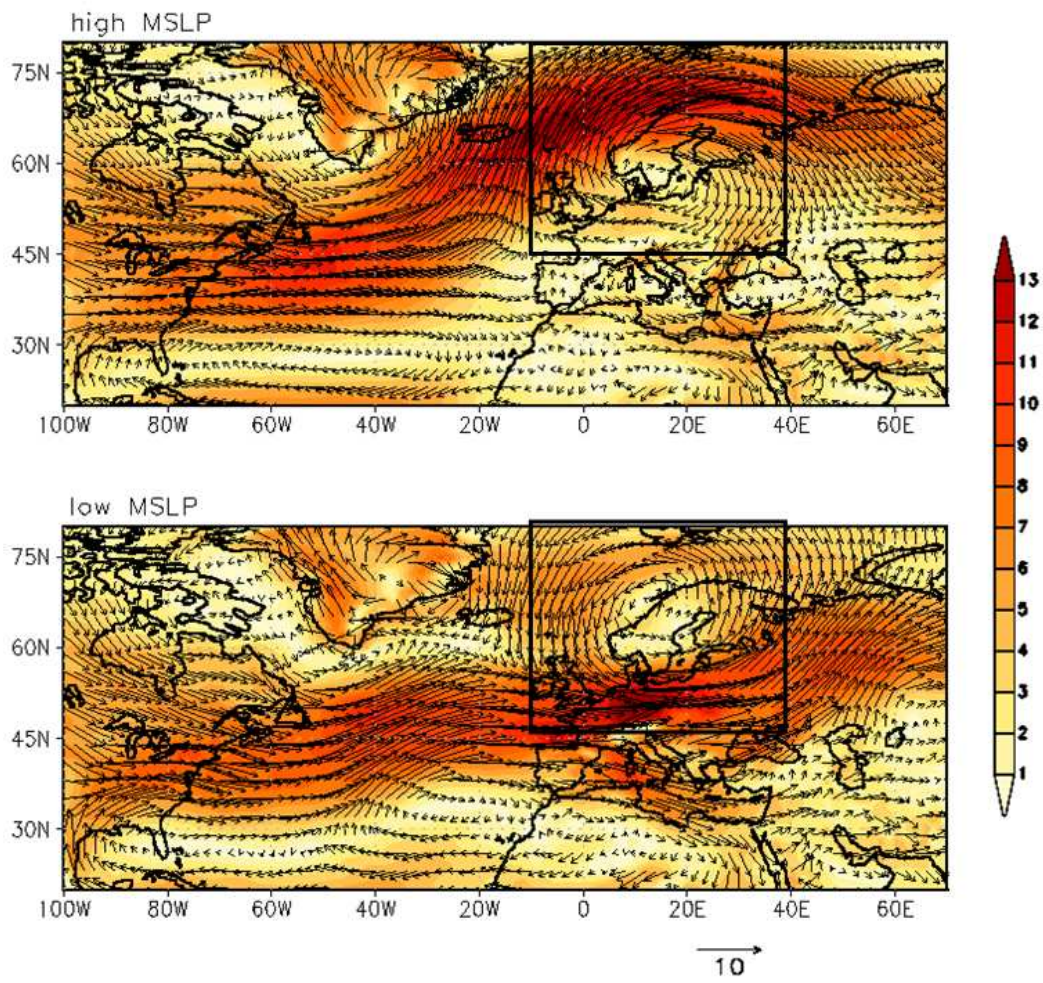
686
 687 Fig. 1: Atmospheric circulation patterns at 850 hPa when winds (in m/s) are NW and NE over the
 688 center of the study area. The colourbar indicates wind strength (in m/s). The study area is marked with
 689 black rectangle.

690
 691
 692
 693
 694
 695
 696
 697
 698
 699
 700
 701
 702
 703
 704
 705
 706
 707
 708



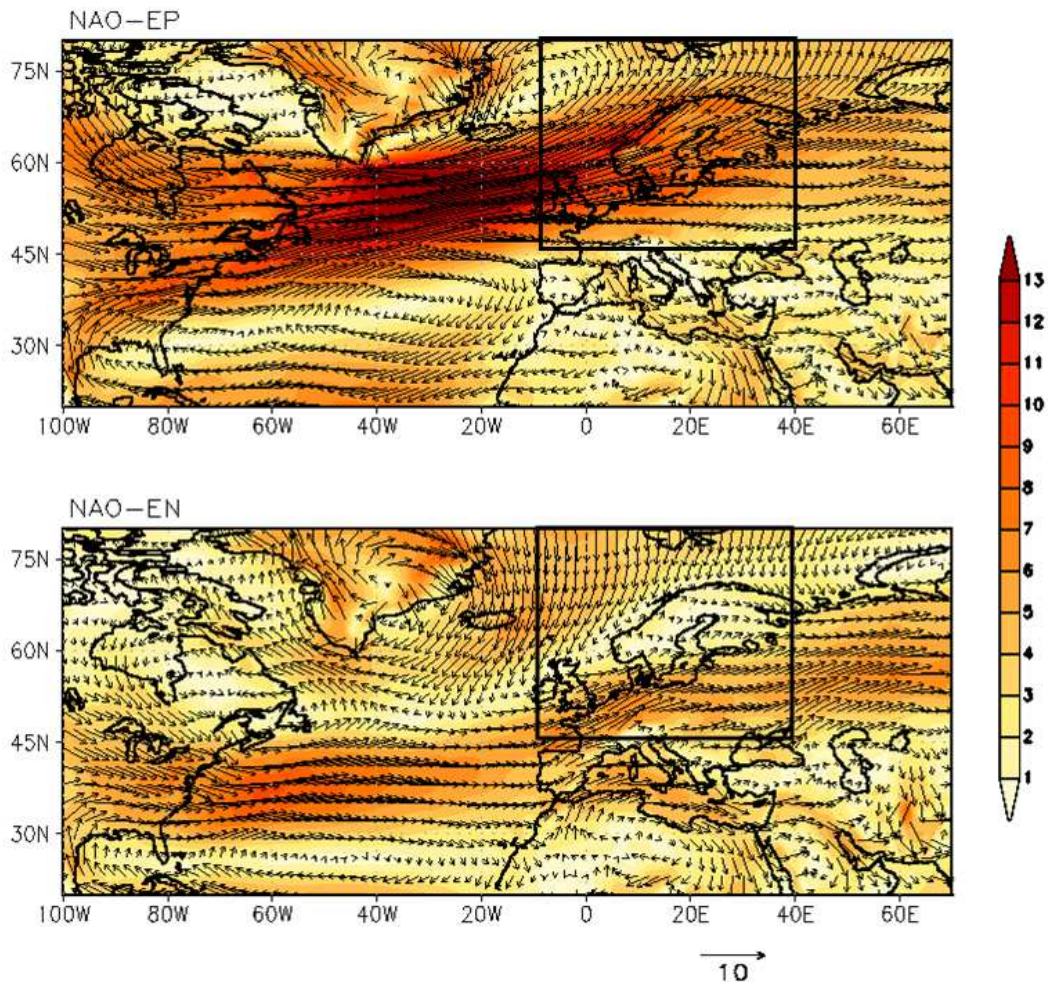
710
711
712
713
714
715
716
717
718
719
720
721
722
723
724
725
726
727
728
729
730
731

Fig. 2: Same as in Fig. 1, but for the SW and SE directions.



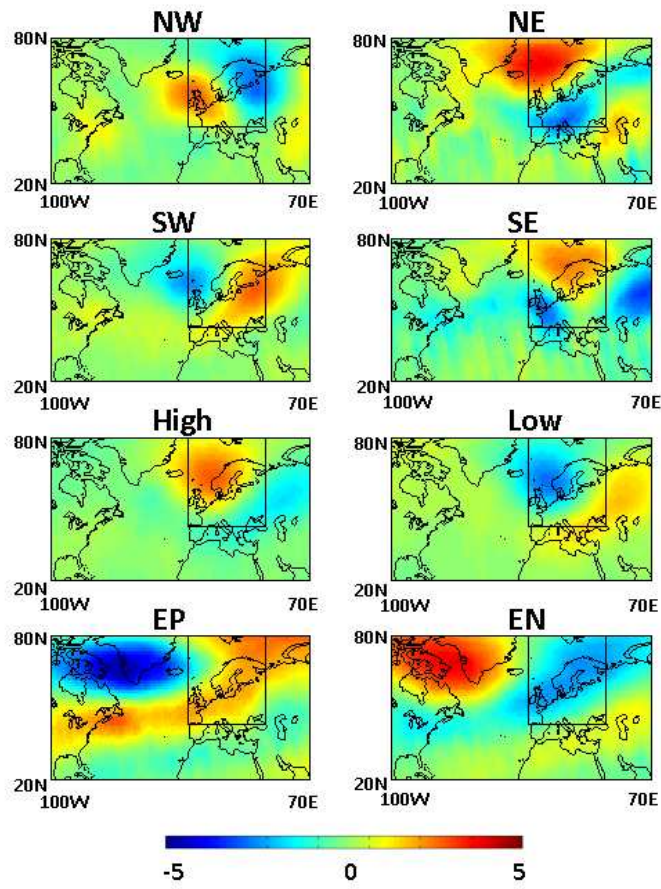
733
734
735
736
737
738
739
740
741
742
743
744
745
746
747
748
749
750
751
752
753
754

Fig. 3: Atmospheric circulation patterns at 850 hPa during high and low MSLP conditions.



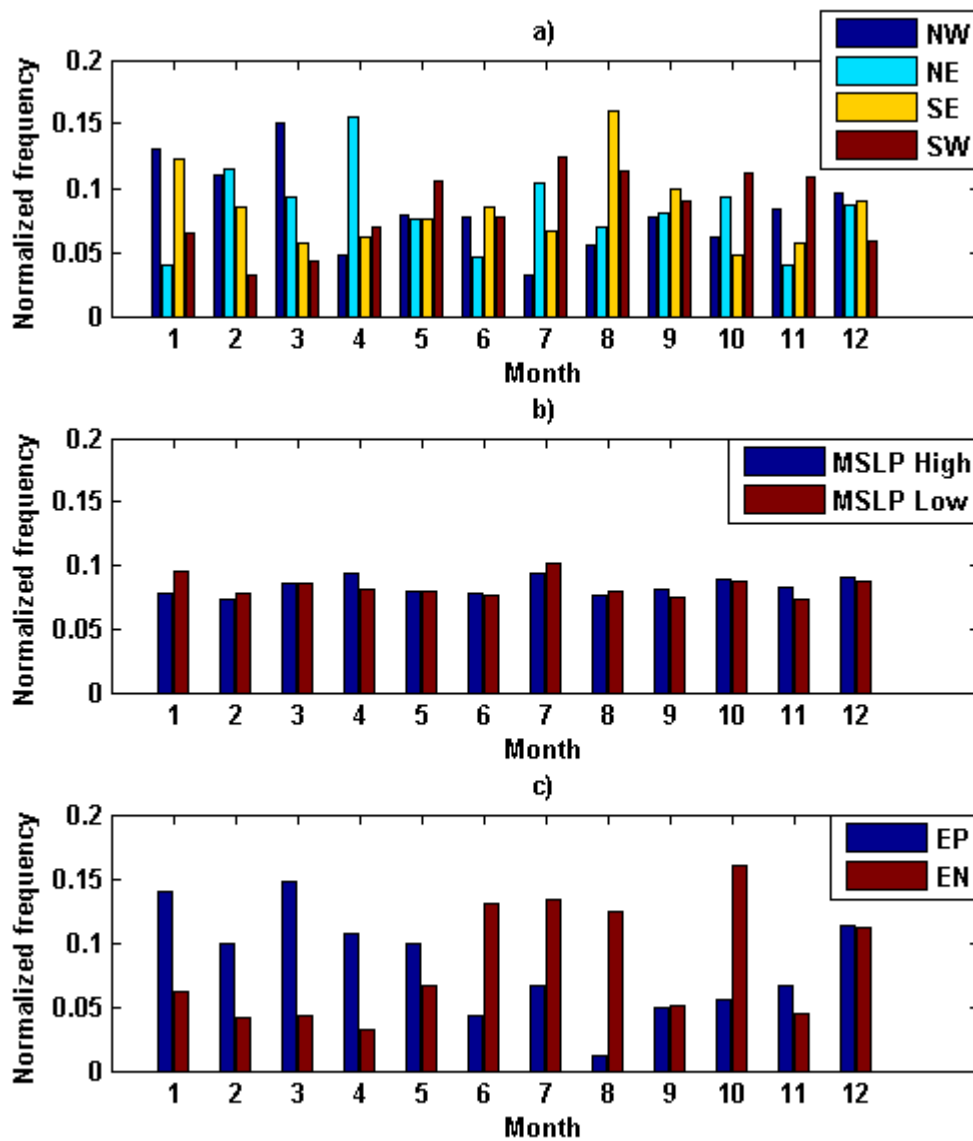
756
757
758
759
760
761
762
763
764
765
766
767
768

Fig. 4: Atmospheric circulation patterns at 850 hPa during enhanced positive and negative phases of NAO.

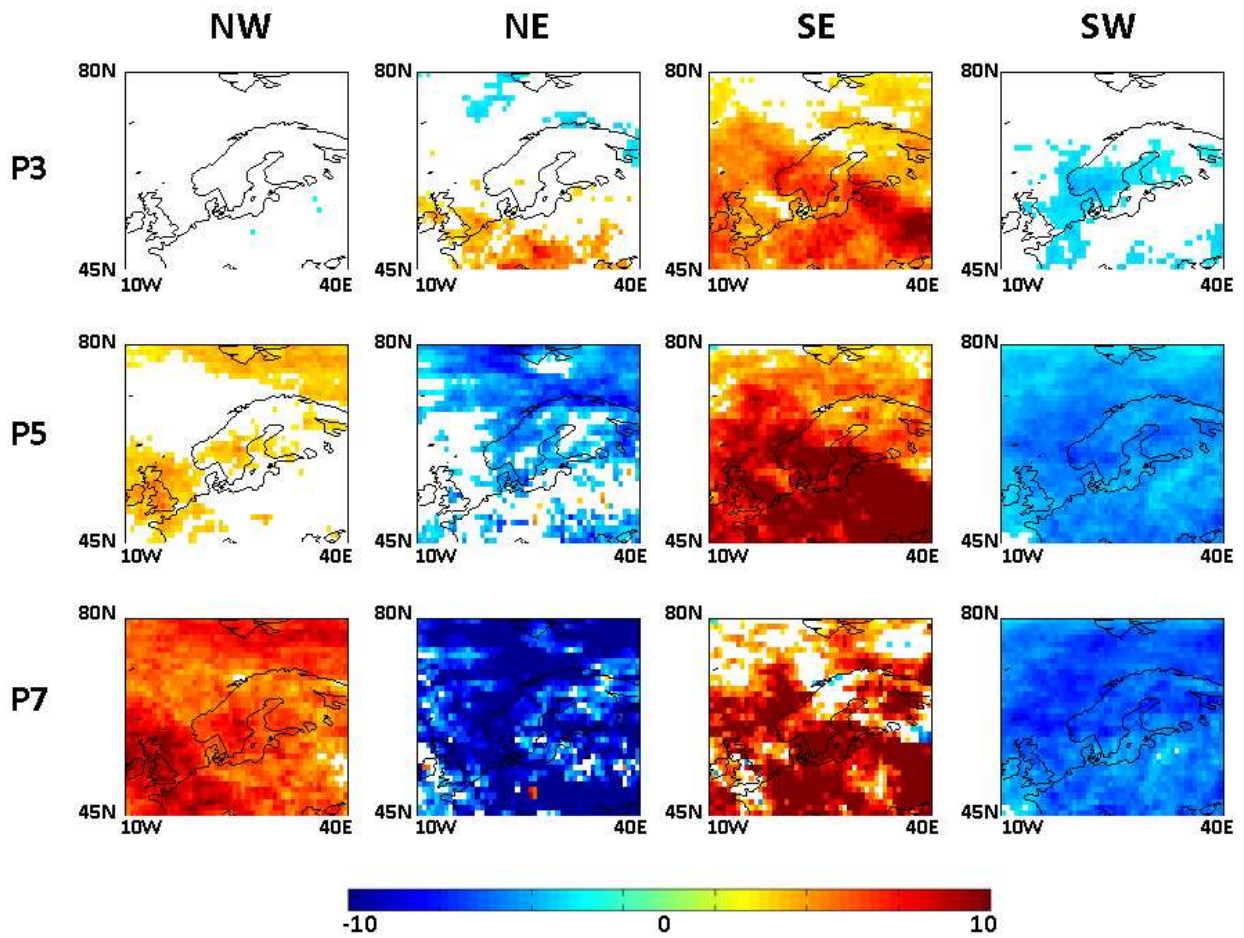


769
 770
 771
 772
 773
 774
 775
 776
 777
 778
 779
 780
 781
 782
 783
 784
 785
 786
 787
 788
 789

Fig. 5: Temperature anomalies at 850 hPa [in K] observed during selected weather states.

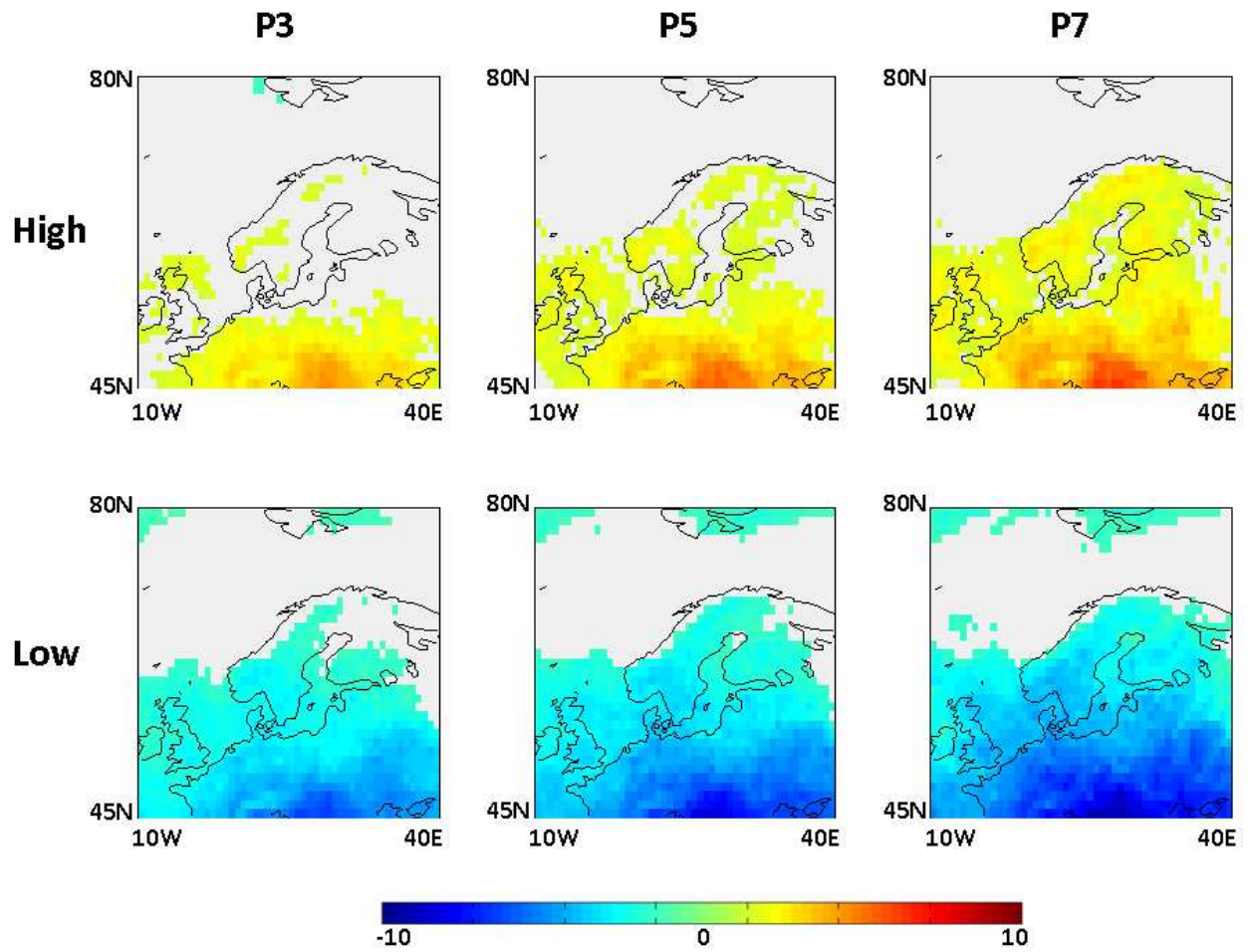


790
 791 Fig. 6: Normalised distribution of the number of weather events as a function of month when they
 792 sustained for 5 days for a) wind directions, b) anticyclonic and cyclonic cases and c) for enhanced
 793 positive and negative NAO.
 794
 795
 796
 797
 798
 799
 800
 801
 802
 803
 804



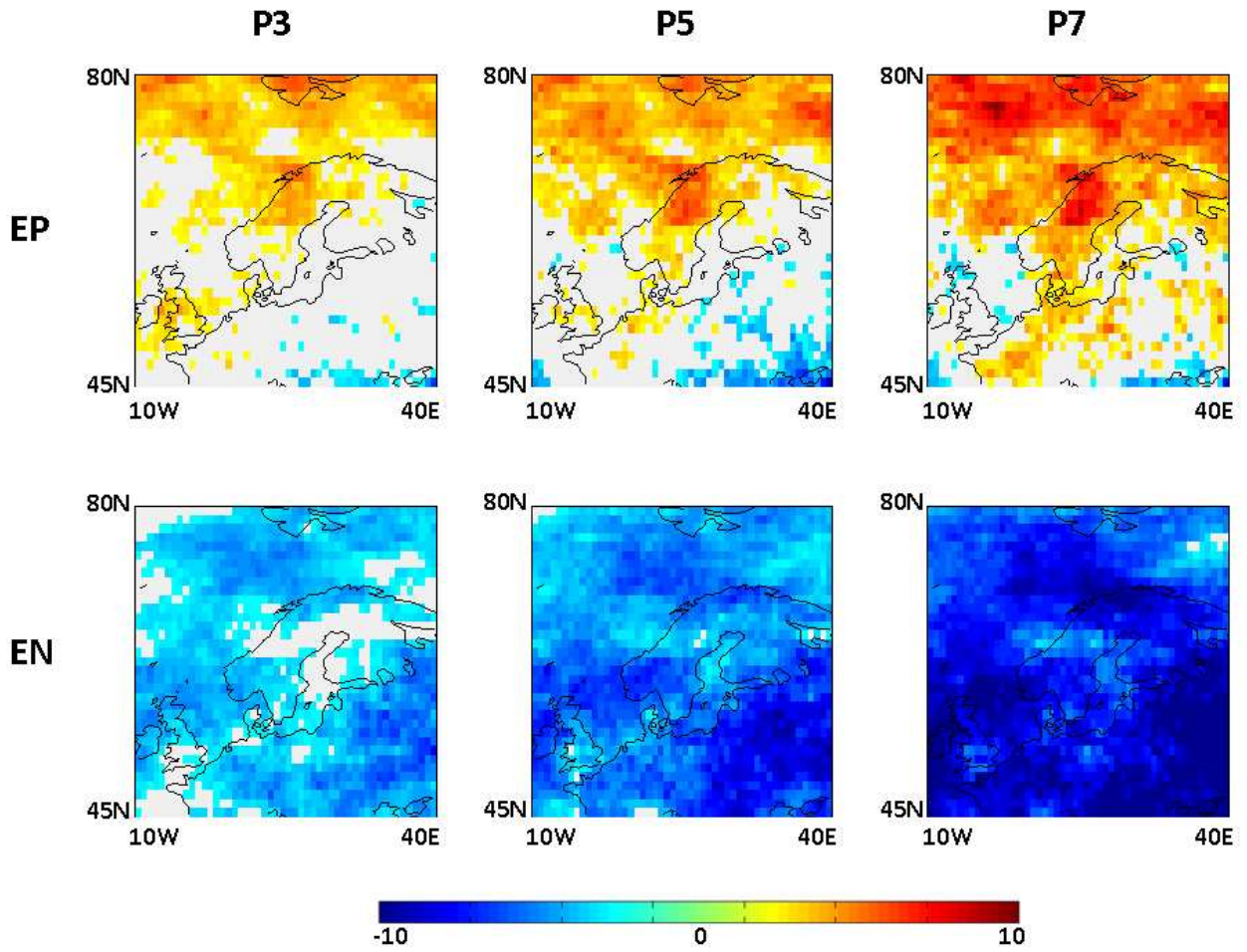
805
 806
 807
 808
 809
 810
 811
 812
 813
 814
 815
 816
 817
 818
 819
 820
 821
 822
 823
 824
 825
 826
 827

Fig. 7: CO anomalies (in ppbv) at 500 hPa observed under different wind conditions and their persistency periods. Only those anomalies exceeding one standard deviation are shown.



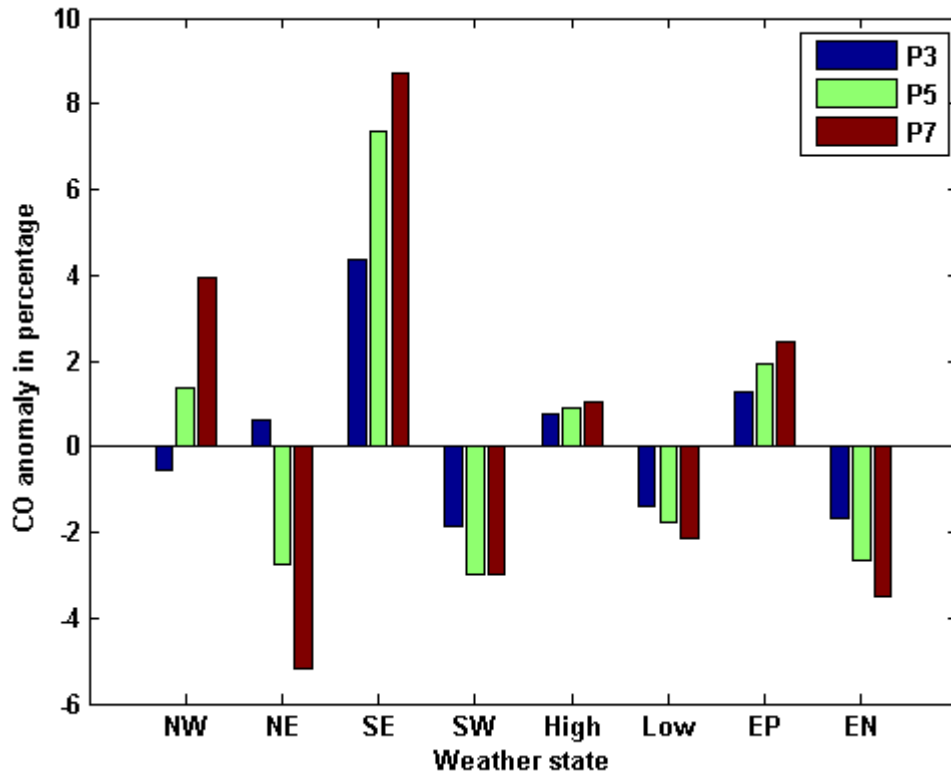
828
 829
 830
 831
 832
 833
 834
 835
 836
 837
 838
 839
 840
 841
 842
 843
 844
 845
 846
 847
 848
 849
 850

Fig. 8: Same as in Fig. 7, but under high and low MSLP conditions and their persistency periods.



852
853
854
855
856
857
858
859
860
861
862
863
864
865
866
867
868
869
870
871
872
873

Fig. 9: Same as in Fig. 7 but under enhanced positive and negative phases of NAO and their persistency periods.



875

876

877 Fig. 10: Percentage increase or decrease in CO at 500 hPa observed during different weather states and
 878 their persistency periods compared to respective weighted climatologies over the study area.

879

880

881

882

883

884

885

886

887

888

889

890

891

892

893

894

895

896

897

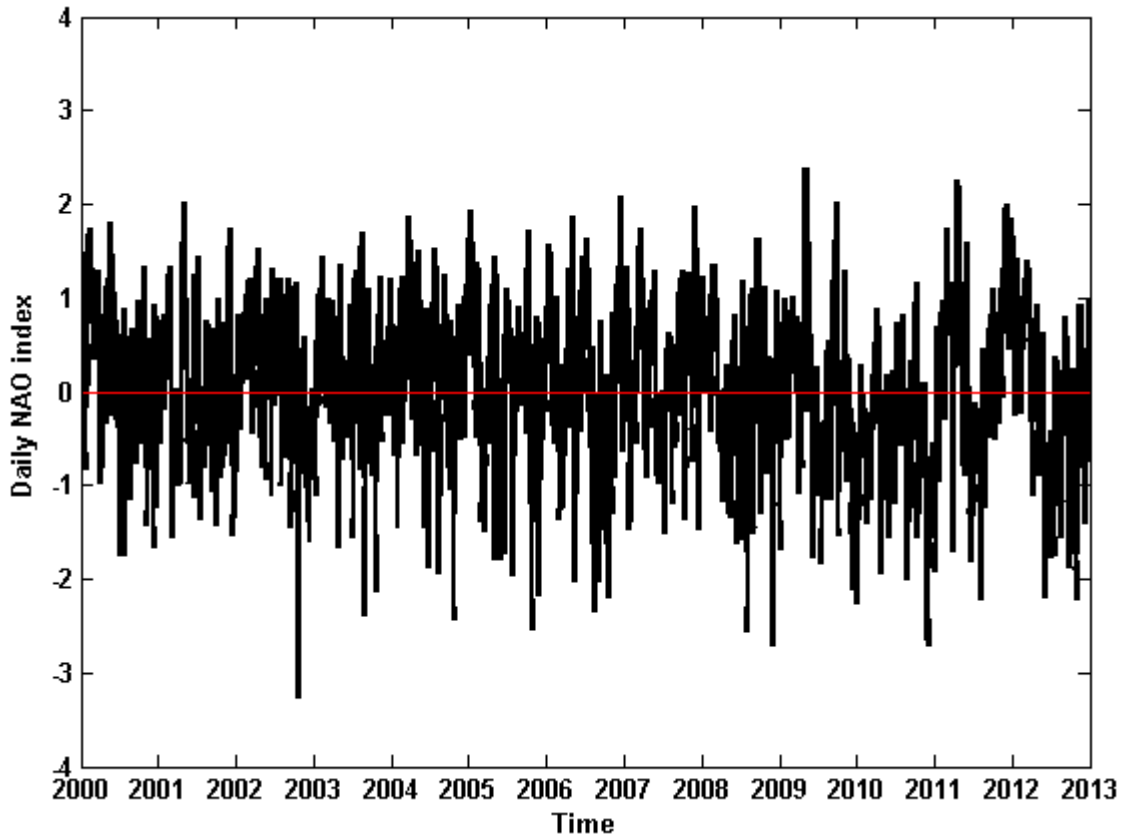
898

899

900

901
902
903
904
905
906
907

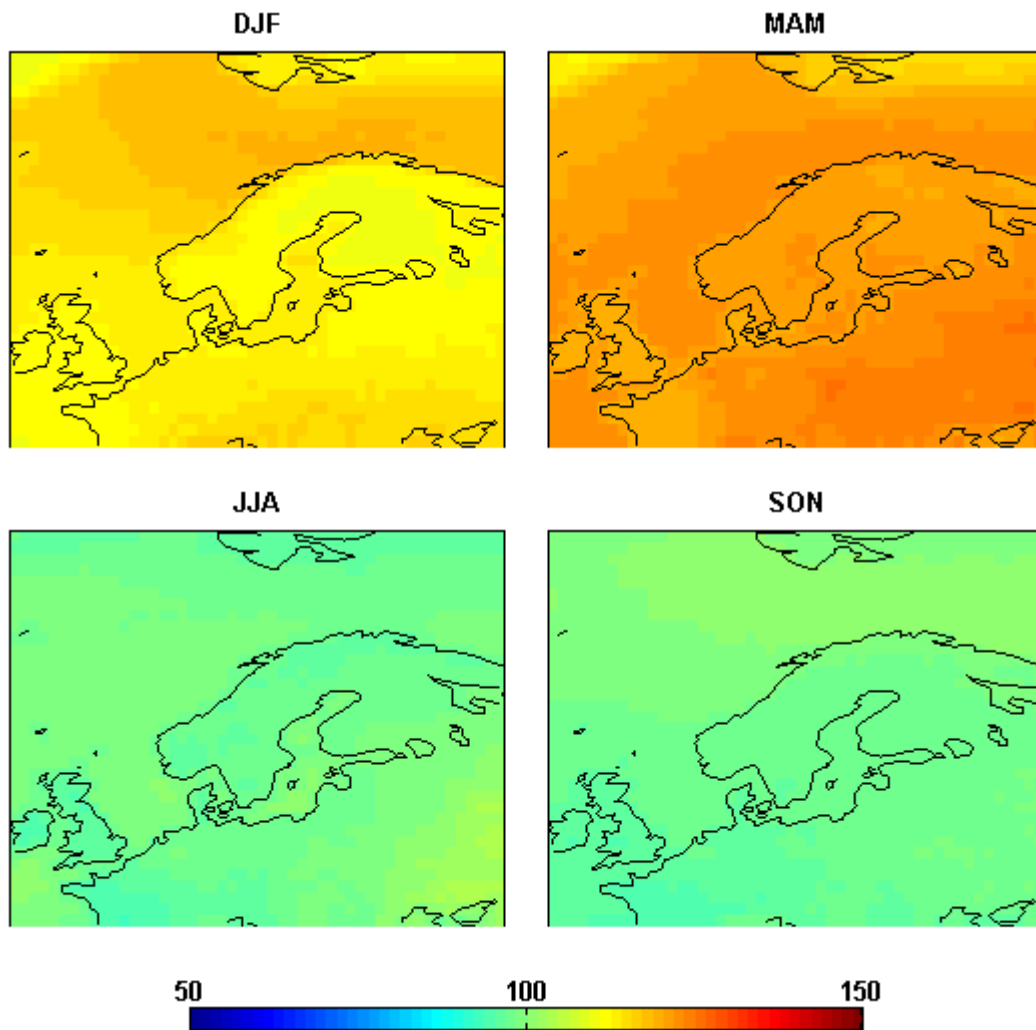
Supplementary figures



908
909
910
911
912
913
914
915
916
917
918
919
920
921
922
923
924
925
926
927

Figure S1: Time series of daily NAO index. The indices are taken from:
<http://www.cpc.ncep.noaa.gov/products/precip/CWlink/pna/nao.shtml>

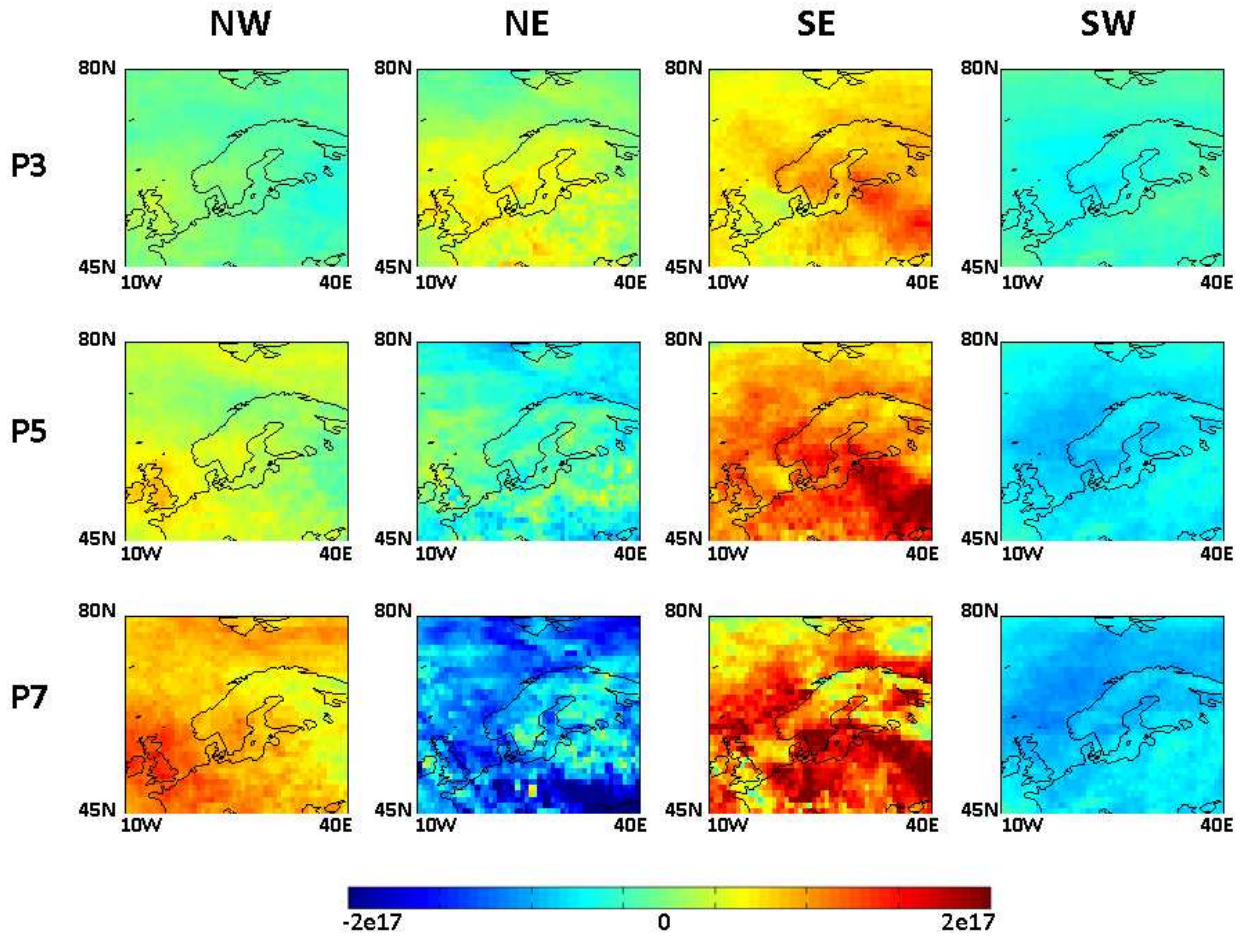
928
929



930
931
932
933
934
935
936
937
938
939
940
941
942
943
944
945
946
947
948

Figure S2: Mean seasonal CO (in ppbv) over the study area at 500 hPa. The entire 11-yr AIRS record is used to compute means.

949
950
951



952
953
954
955
956
957
958
959
960
961
962
963
964
965
966

Figure S4: Total column CO anomalies (in molecules/cm²) under different wind conditions.